Supporting Materials

Enhanced peroxymonosulfate activation by copper-doped bismuth oxides for the efficient photo-degradation of ciprofloxacin: Crucial role of copper sites, theory calculation and mechanism insight

Wei Wang[a, 1], Zhixiong Yang[a, 1], Yuan Li [a], Junting Wang[a] and Gaoke Zhang[a *]

[a] *Hubei Key Laboratory of Mineral Resources Processing and Environment, Key Laboratory of Green Utilization of Critical Non-metallic Mineral Resources, Ministry of Education, State Key Laboratory of Silicate Materials for Architectures, Wuhan University of Technology, 122 Luoshi Road, Wuhan 430070, China*

[1] *These authors contributed equally to this work*

***** *Corresponding author: Gaoke Zhang*

E-mail address: gkzhang@whut.edu.cn (Gaoke Zhang)

Text S1. Reagents

Peroxymonosulfate (PMS), sodium hydroxide (NaOH), ciprofloxacin (CIP), Potassium iodide (KI), Tetracycline (TC), Rhodamine B (RhB), Metronidazole (MNZ), sodium bicarbonate ($NaHCO_3$), sodium persulfate ($Na_2S_2O_8$), bismuth nitrate pentahydrate ($Bi(NO_3)\cdot 5H_2O$), dilute nitric acid (HNO_3), sodium chloride (NaCl), sodium sulfate (Na_2SO_4), sodium nitrate ($NaNO_3$), humic acid (HA), methanol (MA), tert-butyl alcohol (TBA), p-benzoquinone (BQ), L-histidine (L-His), and sodium oxalate ($Na_2C_2O_4$) and copper acetate monohydrate ($Cu(CH_3COO)_2\cdot H_2O$) were purchased from Sinopharm Chemical Reagent Co. Ltd. Sodium bismuthate ($NaBiO_3\cdot 2H_2O$) was synthesized according to the previous study as described in Text S2 of Supporting Material. All reagents did not require further purification.

Text S2. Synthesis of $NaBiO_3\cdot 2H_2O$

20 mM of $Bi(NO_3)_3\cdot 5H_2O$ was added to 50 mL of 1 M HNO_3, and the mixture was stirred for a certain period of time. Subsequently, 18 mM $Na_2S_2O_8$ was introduced, and the solution was stirred for 1 h. Afterward, 10 M NaOH was added, and the solution was thoroughly mixed. The resulting mixture was then heated in a 90°C water bath for 1 h. Finally, the $NaBiO_3$ product was collected by centrifugation after washing with water.

Text S3. Measurement the concentration of PMS

The concentration of PMS in reaction system was detected through a color method of iodine. Specifically, the standard solution of PMS with different concentrations was added into 5 mL solution A containing 0.20 g $NaHCO_3$, 4.00 g KI and 40 mL ultrapure water. After 15 min, the absorbance of mixture solution at λ =352 nm was examined by a UV–vis spectrophotometer for a standard curve. And then, the 1 mL sample was also added into 5 mL solution A and tested with the same procedure.

Text S4. ESR measurements

To investigate the spin trapping ESR spectra of •OH, $SO_4^{\bullet-}$, and $O_2^{\bullet-}$ and $^1O_2$, 2 mg of catalyst and 2 mg of PMS were added to 100 mL of CIP aqueous solution (5 mg/L) to detect •OH and $SO_4^{\bullet-}$ radicals, or to methanol-based CIP solution (5 mg/L) to detect $O_2^{\bullet-}$ radicals. Subsequently, 1 mL of the reaction solution was collected at specific time

intervals, filtered using a 0.22 μm filter, and then 20 μL of 5,5-dimethyl-1-pyrroline N-oxide (DMPO) was added to the filtered solution, shaken for 1 min, and transferred to a capillary tube for EPR detection. To detect $^1O_2$, 100 μL of 2,2,6,6-Tetramethylpiperidine (TEMP) was added to the filtered solution, shaken for 1 min, and then analyzed in a capillary tube.

Text S5. Theory calculations

Density functional theory (DFT) calculations were carried out using the Vienna Ab-initio Simulation Package (VASP) with the Projector Augmented Wave (PAW) method.[1,2] A cutoff energy of 400 eV was used for the plane-wave basis. Surface atoms were allowed to relax until forces were below 2×10^{-2} eV/Å, and the energy change per atom was under 10^{-5} eV/atom, completing both ionic and electronic relaxations. To eliminate periodic boundary effects, a 20 Å vacuum layer was added in the z-axis. Additionally, we employed the DFT+U method to address the localized nature of Cu 3d electrons in the Cu-doped BiO_{2-x} system, with a U value of 4.0 eV for the Cu 3d orbitals. [3,4] The adsorption energies of PMS on the catalyst surface were calculated using Eq. 1:

$$E_{ads} = E_{catalyst/PMS} - E_{PMS} - E_{catalyst} \quad (1)$$

where $E_{catalyst/PMS}$, E_{PMS}, and $E_{catalyst}$ represent the total energy of PMS adsorbed on the catalyst, free PMS, and the catalyst itself, respectively.

DFT calculations by Gaussian 09 software at B3LYP/6-31+G**= (d, p) level was performed to figure out the nucleophilic and electrophilic attack on the molecular structure of CIP. Based on the wave function, Multiwfn 3.8 software was used to analyze the visualization of the highest occupied molecular orbital (HOMO), calculated DD (b) and f, and Fukui index.[5,6]

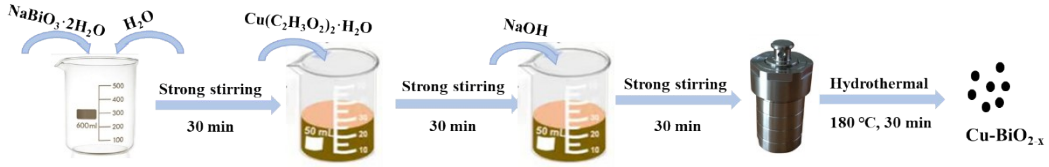

Fig. S1. Schematic diagram of preparing Cu doped BiO_{2-x}.

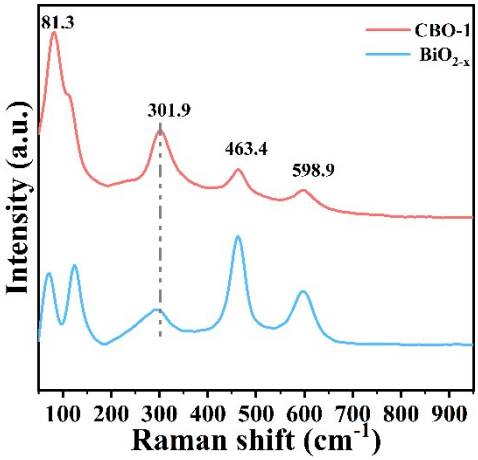

Fig. S2. Raman spectra of BiO_{2-x} and CBO-1.

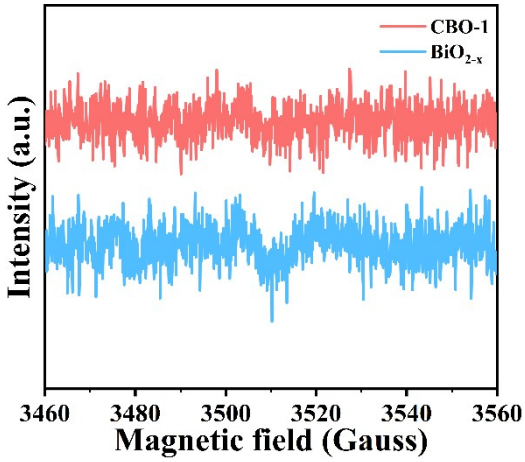

Fig. S3. ESR spectra of BiO_{2-x} and CBO-1.

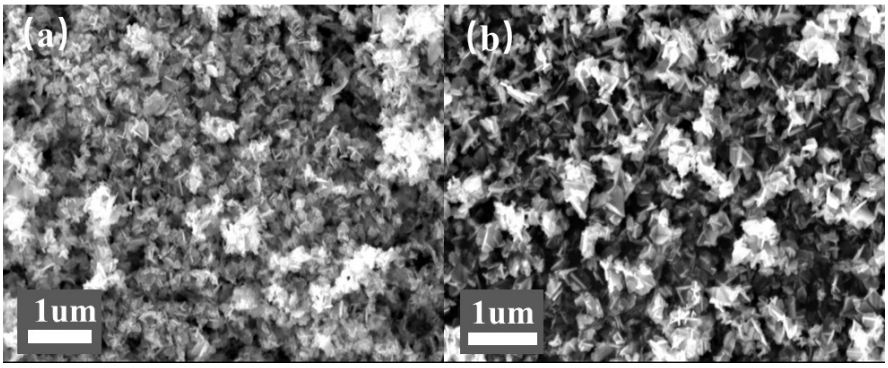

Fig. S4. SEM images of (a) BiO_{2-x} and (b) CBO-1.

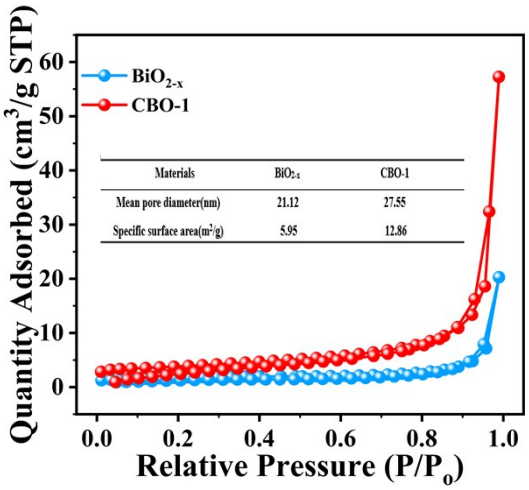

Fig. S5. BET spectra of BiO_{2-x} and CBO-1.

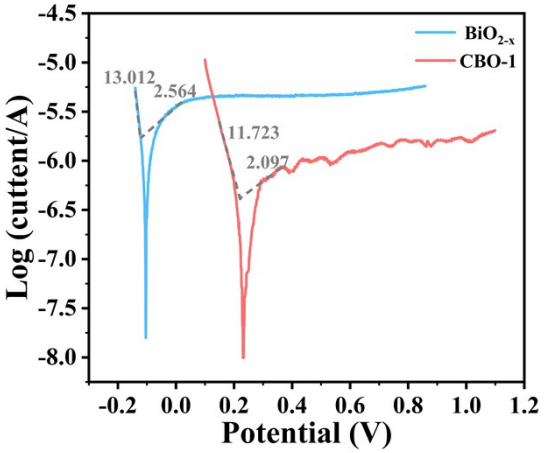

Fig. S6. Tafel curves of BiO_{2-x} and CBO-1.

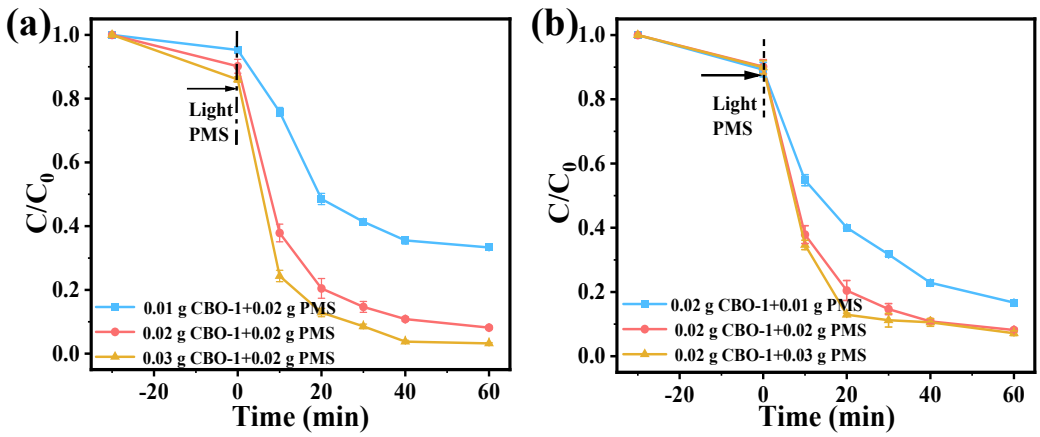

Fig. S7. (a) Effect of different dosages of CBO-1, (b) PMS concentration on the CIP degradation in the CBO-1/PMS/Vis system.

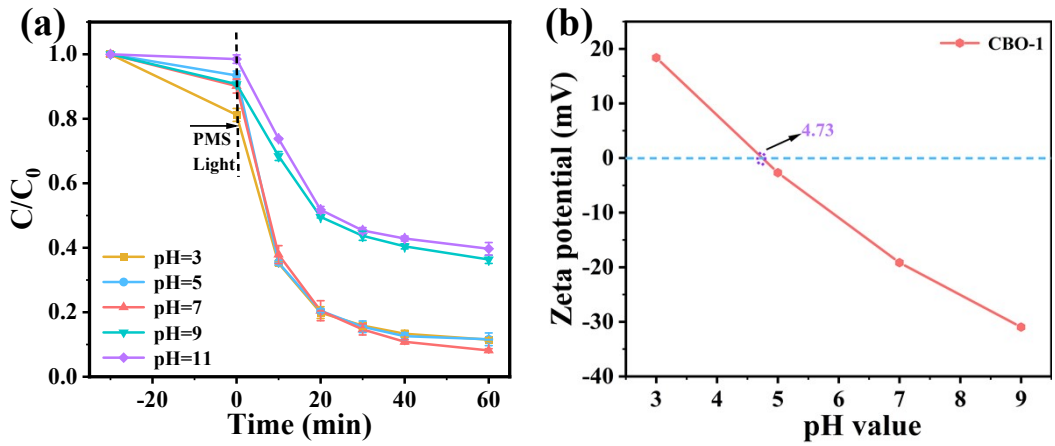

Fig. S8. (a) Effect of initial pH on the CIP degradation in the CBO-1/PMS/Vis system and (b) Zeta potential of CBO-1 at different pH levels**.**

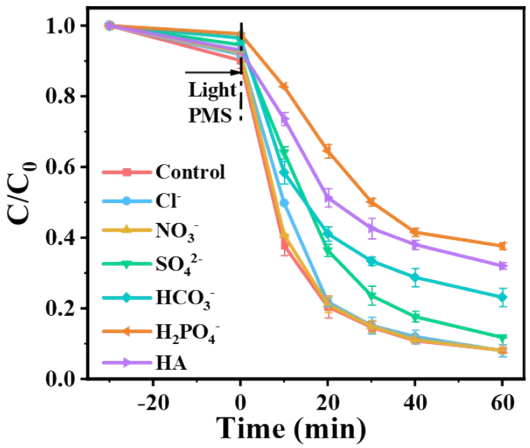

Fig. S9. Effect of inorganic anions and dissolved organic matter on the CIP degradation in the CBO-1/PMS/Vis system.

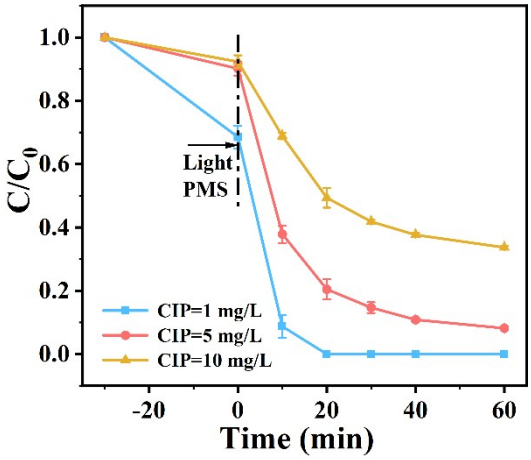

Fig. S10. CIP concentration in CBO-1/PMS/Vis system with different initial CIP concentrations.

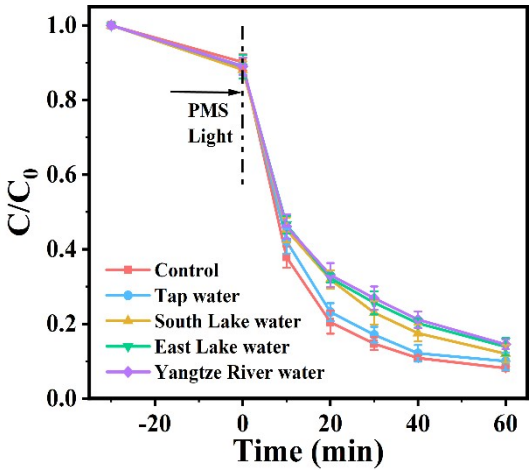

Fig. S11. Efficiency of CBO-1/PMS/Vis degradation of CIP under actual water environment background.

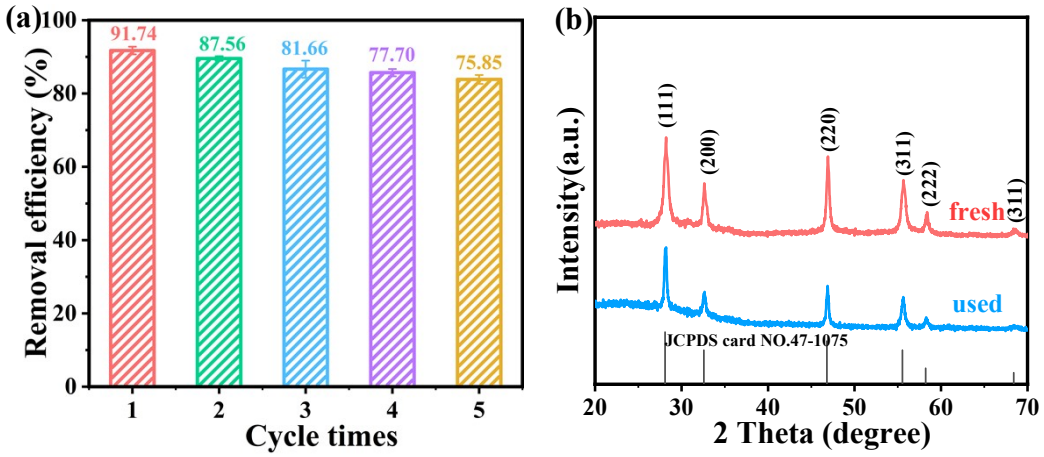

Fig. S12. (a) Cycle experiments of CIP degradation in CBO-1/PMS/Vis system and (b) XRD patterns of fresh and used (five cycles) CBO-1.

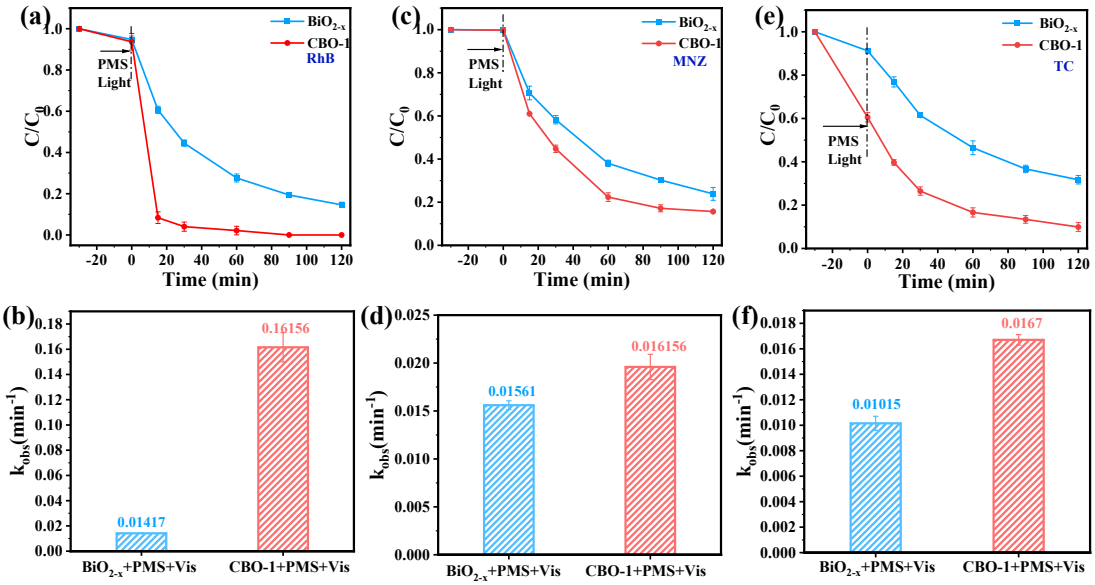

Fig. S13. (a) Degradation of RhB and (b) their corresponding reaction kinetics under CBO-1/Vis system and BiO_{2-x}/Vis system. (c) Degradation of MNZ and (d) their corresponding reaction kinetics under CBO-1/Vis system and BiO_{2-x}/Vis system. (e) Degradation of TC and (f) their corresponding reaction kinetics under CBO-1/Vis system and BiO_{2-x}/Vis system.

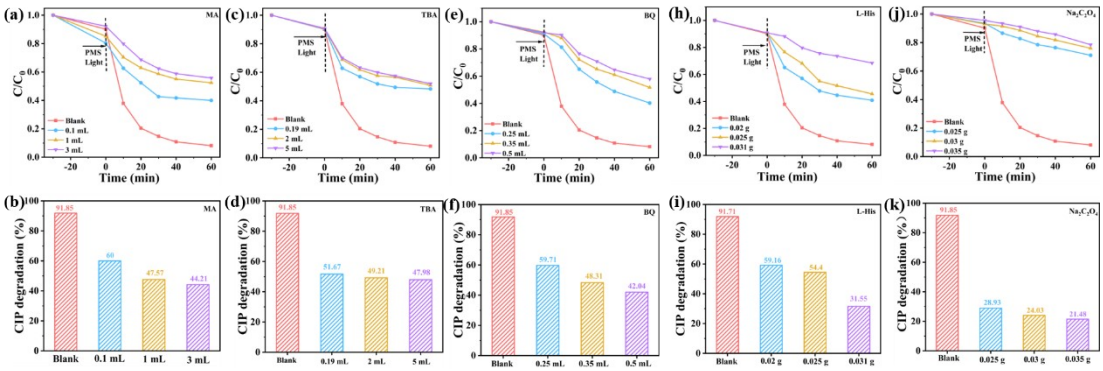

Fig. S14. In the CBO-1/PMS/Vis system, the degradation curves of CIP by different concentrations of quenchers are shown as follows: (a) methanol, (c) n-butanol, (e) p-benzoquinone, (h) L-histidine, and (j) sodium oxalate, and corresponding degradation rate graphs: (b) methanol, (d) n-butanol, (f) p-benzoquinone, (i) L-histidine, and (k) sodium oxalate.

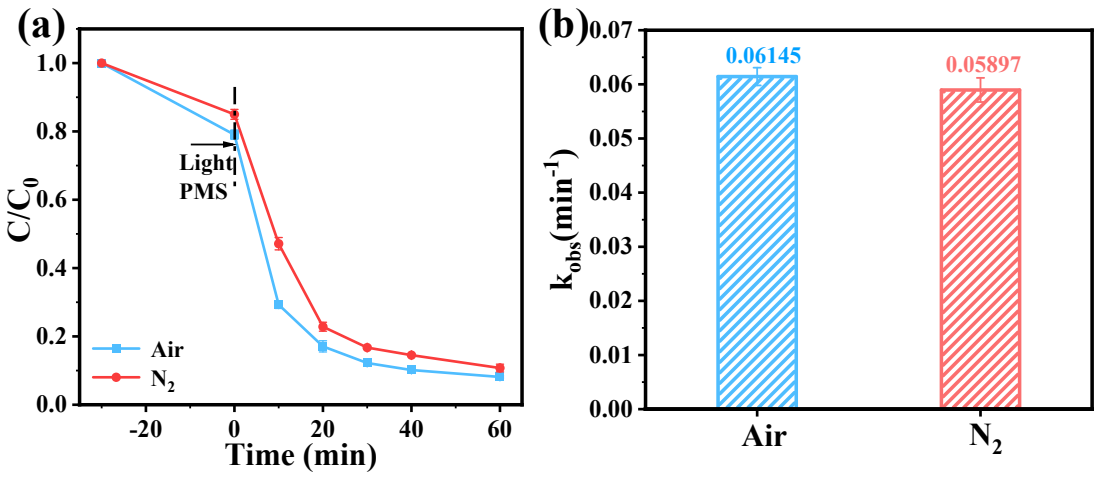

Fig. S15. (a) CIP degradation by CBO-1/PMS/Vis system in different atmosphere and (b) their corresponding reaction kinetics.

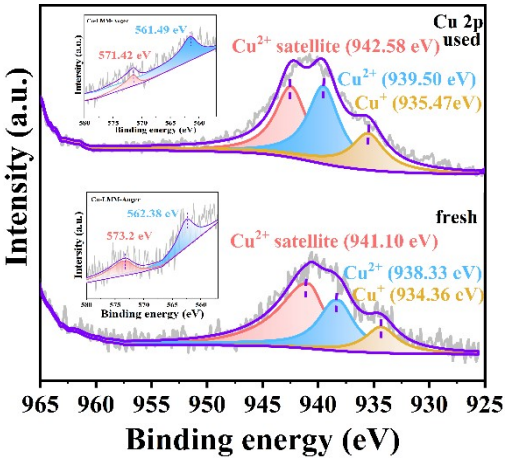

Fig. S16. HR-XPS spectra of Cu 2p (insect: Auger spectrum of Cu) of fresh and used CBO-1.

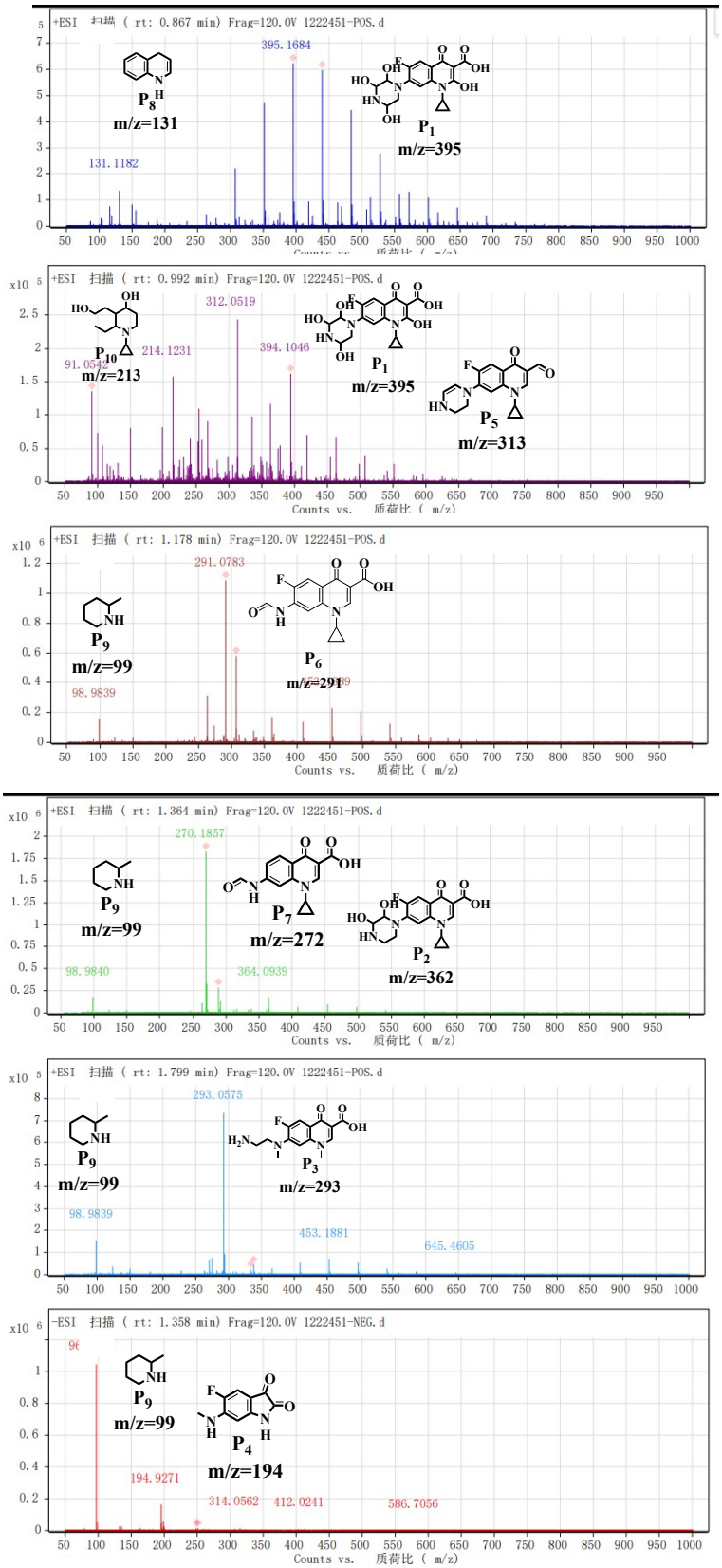

Fig. S17. Mass spectrum of the identified intermediates of CIP degradation.

Table S1. Comparative studies on the photocatalytic degradation performance of CIP by photoactivated PMS

Samples	Reaction conditions	Light source	Degradation rate	Ref.
Cu doped BiO_{2-x}	CIP: 5 mg/L, 100 mL; Photocatalyst: 0.2 g/L; PMS: 0.2 g/L	420 nm; 100 W	0.0607 min^{-1}	This work
$BiVO_4$	CIP: 10 mg/L, 100 mL; Photocatalyst: 0.32 g/L; PMS: 0.96 g/L	⩾420 nm;	0.0565 min^{-1}	7
$Cu_{0.84}Bi_{2.08}O_4$	CIP: 40 mg/L, 40 mL; Photocatalyst: 1 g/L; PDS: 1 mM	420 nm; Xenon lamp; 300 W	0.0102 min^{-1}	8
$BiO_{1-x}Br$/ $Bi_2O_2CO_3$	CIP: 40 mg/L, 50 mL; Photocatalyst: 1 g/L	420 nm; Xenon lamp; 500 W	0.01551 min^{-1}	9
$C_3N_4/MnFe_2O_4$-G	CIP: 20 mg/L, 50 mL; Photocatalyst: 1 g/L; PS: 10 mM	400 nm; Xenon lamp; 300 W	0.043 min^{-1}	10
MIL-68(In,Bi)-NH_2@BiOBr	CIP: 10 mg/L, 100 mL; Photocatalyst: 0.25 g/L;	⩾420 nm; Xenon lamp; 300 W	0.02516 min^{-1}	11
BiOBr	CIP: 5 mg/L, 40 mL; Photocatalyst: 0.5 g/L;	420 nm; Halogen lamp ; 400 W	0.0272 min^{-1}	12
g-C_3N_4/Ti_3C_2	CIP: 20 mg/L, 50 mL; Photocatalyst: 0.2 g/L;	Xenon lamp; 500 W	0.035 min^{-1}	13

Co doped BiOCl	BPA: 10 mg/L, 30 mL; Photocatalyst: 0.2 g/L	⩾420 nm; Xenon lamp; 500 W	0.021 min^{-1}	14
Cu doped BiO_{2-x}	BPA: 50 mg/L, 100 mL; Photocatalyst: 0.75 g/L	770-860 nm; 100 W	0.047 min^{-1}	15
$Bi_2O_4/Bi_4O_7/BiO_{2-x}$	BPA: 40 mg/L, 40 mL; Photocatalyst: 0.4 g/L	850 nm; LED light; 100 W	0.0081 min^{-1}	16
$BiOI/TiO_2$	CIP: 1 mg/L, 30 mL; Photocatalyst: 1 g/L; PMS: 0.25 mM	⩾420 nm; Xenon lamp; 500 W	0.023 min^{-1}	17

Reference

[1] G. Kresse, J. Furthmüller, Efficient iterative schemes for ab initio total-energy calculations using a plane-wave basis set, Phys. Rev. B., 1996, 54, 11169. https://doi.org/10.1103/physrevb.54.11169.

[2] P.J. Stephens, F. J. Devlin, C. F. Chabalowski, M. J. Frisch, Ab Initio calculation of vibrational absorption and circular dichroism spectra using density functional force fields, J. Phys. Chem., 1994, 98, 11623–11627. https://doi.org/ 10.1021/j100096a001.

[3] Y. Zhang, Advancing DFT predictions in Cu-chalcogenides with full-yet-shallow 3*d*-orbitals: Meta-GGA plus Hubbard-like *U* correction, J. Chem. Phys., 2024, 161, 174109. https://doi.org/10.1063/5.0232711.

[4] Y. Zhang, X. Yuan, X. Sun, B.-C. Shih, P.Zhang, and W. Zhang, Comparative study of structural and electronic properties of Cu-based multinary semiconductors, *Phys. Rev. B.*, 2011, 84, 075127. https://doi.org/10.1103/physrevb.84.075127.

[5] V. Springer, M.A. Segundo, M.E. Centurion and M. Avena, Fully-programmable synthesis of sucrose-mediated gold nanoparticles for detection of ciprofloxacin, Mater. Chem. Phys., 2019, 238, 121917. https://doi.org/10.1016/j.matchemphys.2019.121917.

[6] T. Lu and F. Chen, multiwfn: a multifunctional wavefunction analyzer, J. Comput. Chem., 2012, 33, 580–59. https://doi.org/10.1246/bcsj.67.1085.

[7] F. Chen, G. Huang, F. Yao, Q. Yang, Y. Zheng, Q. Zhao, H. Yu, Catalytic degradation of ciprofloxacin by a visible-light-assisted peroxymonosulfate activation system: Performance and mechanism, Water Res., 2020, 173, 115559. https://doi.org/10.1016/j.watres.2020.115559.

[8] H. Tang, Z. Dai, X. Xie, Z. Wen, R. Chen, Promotion of peroxydisulfate activation over $Cu_{0.84}Bi_{2.08}O_4$ for visible light induced photodegradation of ciprofloxacin in water matrix, Chem. Eng. J., 2019, 356, 472–482. https://doi.org/10.1016/j.cej.2018.09.066.

[9] J. Ding, Z. Dai, F. Qin, H. Zhao, S. Zhao, R. Chen, Z-scheme $BiO_{1-x}Br/Bi_2O_2CO_3$ photocatalyst with rich oxygen vacancy as electron mediator for highly efficient degradation of antibiotics, Appl. Catal. B-Environ., 2017, 205, 281–291. https://doi.org/10.1016/j.apcatb.2016.12.018.

[10] X. Wang, A. Wang, J. Ma, Visible-light-driven photocatalytic removal of antibiotics by newly designed C_3N_4@$MnFe_2O_4$-graphene nanocomposites, J. Hazard. Mater., 2017, 336, 81–92. https://doi.org/10.1016/j.jhazmat.2017.04.012.

[11] Y. Peng, J. Lin, J.-L. Niu, X. Guo, Y. Chen, T. Hu, J. Cheng, Y. Hu, Synergistic effect of ion doping and type-II heterojunction construction and ciproffoxacin degradation by MIL-68(In, Bi)-NH2@BiOBr under visible light, ACS Appl. Mater. Interfaces., 2024, 16 (2), 2351–2364. https://doi.org/10.1021/acsami.3c16037.

[12] X. Zhang, R. Li, M. Jia, S. Wang, Y. Huang, C. Chen, Degradation of ciprofloxacin in aqueous bismuth oxybromide (BiOBr) suspensions under visible light irradiation: a direct hole oxidation pathway, Chem. Eng. J., 2015, 274, 290–297. https://doi.org/10.1016/j.cej.2015.03.077.

[13] N. Liu, N. Lu, Y. Su, P. Wang, X. Quan, Fabrication of g-C_3N_4/Ti_3C_2 composite and its visible-light photocatalytic capability for ciprofloxacin degradation, Sep. Purif. Technol., 2019, 211, 782-789. https://doi.org/10.1016/j.seppur.2018.10.027.

[14] C. Wang, Y. Zhang, W. Wang, D. Pei, G. Huang, J. Chen, X. Zhang, H. Yu, Enhanced photocatalytic degradation of bisphenol A by Co-doped BiOCl nanosheets under visible light irradiation, Appl. Catal. B: Environ., 2018, 221, 320-328. https://doi.org/10.1016/j.apcatb.2017.09.036.

[15] Z. Yang, H. Wang, Y. Li, G. Zhang, In-suit generated Cu-ligand inducing full-spectrum selective photocatalytic degradation of organic pollutants containing phenol groups over Cu doping BiO_{2-x} nanosheet: The synergistic effects of Cu-ligand and oxygen vacancies, and mechanism study, Chem. Eng. J., 2024. 499. 155810. https://doi.org/10.1016/j.cej.2024.155810.

[16] Y. Jia, S. Li, H. Ma, J. Gao, G. Zhu, F. Zhang, J. Park, S. Cha, J. Bar, C. Liu, Oxygen vacancy rich Bi_2O_4-Bi_4O_7-BiO_{2-x} composites for UV–vis-NIR activated high efficient photocatalytic degradation of bisphenol A, J. Hazard. Mater., 2020, 382, 121121. https://doi.org/10.1016/j.jhazmat.2019.121121.

[17] X. Chen, J. Yao, H. Dong, M. Hong, N. Gao, Z. Zhang, W. Jiang, Enhanced bezaffbrate degradation and power generation via the simultaneous PMS activation in visible light photocatalytic fuel cell, Water Res., 2021, 207, 117800. https://doi.org/10.1016/j.watres.2021.117800.